

# CEBAF Program Advisory Committee Nine Proposal Cover Sheet

This proposal must be received by close of business on Thursday, December 1, 1994 at:

CEBAF  
User Liaison Office, Mail Stop 12 B  
12000 Jefferson Avenue  
Newport News, VA 23606

## Proposal Title

Longitudinal and Transverse Cross Sections in the  $d(e, e'K^+)_{YN}$  Reactions at  $Q^2 = 0.5$  to  $2$  (GeV/c)<sup>2</sup>

## Contact Person

**Name:** Shelton Y. Beedoe  
**Institution:** North Carolina A & T State University  
**Address:** Dept. of Physics  
**Address:** 101 Marteen Hall  
**City, State ZIP/Country:** Greensboro, NC 27411  
**Phone:** (910)334-7647, 334-7733 **FAX:** (910)334-7283  
**E-Mail → Internet:** beedoes@DIANA, BEEDOE@cebaf.gov

**Experimental Hall:**   c   **Days Requested for Approval:**   27  

**Hall B proposals only, list any experiments and days for concurrent running:**

## CEBAF Use Only

**Receipt Date:**   12/15/94     PR 94-111  

**By:**                     gp

# BEAM REQUIREMENTS LIST

CEBAF Proposal No.: \_\_\_\_\_ Date: \_\_\_\_\_  
(For CEBAF User Liaison Office use only.)

List all combinations of anticipated targets and beam conditions required to execute the experiment. (This list will form the primary basis for the Radiation Safety Assessment Document (RSAD) calculations that must be performed for each experiment.)

Condition #	Beam Energy (MeV)	Beam Current (μA)	Polarization and Other Special Requirements (e.g., time structure)	Target Material (use multiple rows for complex targets — e.g., w/windows)	Target Material Thickness (mg/cm <sup>2</sup> )
	2,400	10		LD <sub>2</sub>	10
	3200	10		LD <sub>2</sub>	"
	4000	5		LD <sub>2</sub>	"
	2400	40		ED <sub>2</sub>	"
	3200	20		LD <sub>2</sub>	"
	4000	30		LD <sub>2</sub>	
	2400	60		LD <sub>2</sub>	"
	3200	60		LD <sub>2</sub>	"
	2400	40		LD <sub>2</sub>	"
	3500	60		LD <sub>2</sub>	"
	4000	60		LD <sub>2</sub>	"

The beam energies,  $E_{\text{Beam}}$ , available are:  $E_{\text{Beam}} = N \times E_{\text{Linac}}$  where  $N = 1, 2, 3, 4,$  or  $5$ . For 1995,  $E_{\text{Linac}} = 800$  MeV, i.e., available  $E_{\text{Beam}}$  are 800, 1600, 2400, 3200, and 4000 MeV. Starting in 1996, in an evolutionary way (and not necessarily in the order given) the following additional values of  $E_{\text{Linac}}$  will become available:  $E_{\text{Linac}} = 400, 500, 600, 700, 900, 1000, 1100,$  and  $1200$  MeV. The sequence and timing of the available resultant energies,  $E_{\text{Beam}}$ , will be determined by physics priorities and technical capabilities.

# HAZARD IDENTIFICATION CHECKLIST

CEBAF Proposal No.: \_\_\_\_\_  
(For CEBAF User Liaison Office use only.)

Date: \_\_\_\_\_

Check all items for which there is an anticipated need.

<p><b>Cryogenics</b></p> <p>_____ beamline magnets</p> <p>_____ analysis magnets</p> <p><input checked="" type="checkbox"/> target</p> <p>type: <u>LD<sub>2</sub>, LH<sub>2</sub></u></p> <p>flow rate: _____</p> <p>capacity: _____</p>	<p><b>Electrical Equipment</b></p> <p>_____ cryo/electrical devices</p> <p>_____ capacitor banks</p> <p>_____ high voltage</p> <p>_____ exposed equipment</p>	<p><b>Radioactive/Hazardous Materials</b></p> <p>List any radioactive or hazardous/toxic materials planned for use:</p> <p>_____</p> <p>_____</p> <p>_____</p>
<p><b>Pressure Vessels</b></p> <p>_____ inside diameter</p> <p>_____ operating pressure</p> <p>_____ window material</p> <p>_____ window thickness</p>	<p><b>Flammable Gas or Liquids</b></p> <p>type: _____</p> <p>flow rate: _____</p> <p>capacity: _____</p> <p><b>Drift Chambers</b></p> <p>type: _____</p> <p>flow rate: _____</p> <p>capacity: _____</p>	<p><b>Other Target Materials</b></p> <p>_____ Beryllium (Be)</p> <p>_____ Lithium (Li)</p> <p>_____ Mercury (Hg)</p> <p>_____ Lead (Pb)</p> <p>_____ Tungsten (W)</p> <p>_____ Uranium (U)</p> <p>_____ Other (list below)</p> <p>_____</p> <p>_____</p>
<p><b>Vacuum Vessels</b></p> <p>_____ inside diameter</p> <p>_____ operating pressure</p> <p>_____ window material</p> <p>_____ window thickness</p>	<p><b>Radioactive Sources</b></p> <p>_____ permanent installation</p> <p>_____ temporary use</p> <p>type: _____</p> <p>strength: _____</p>	<p><b>Large Mech. Structure/System</b></p> <p>_____ lifting devices</p> <p>_____ motion controllers</p> <p>_____ scaffolding or</p> <p>_____ elevated platforms</p>
<p><b>Lasers</b></p> <p>type: _____</p> <p>wattage: _____</p> <p>class: _____</p> <p><b>Installation:</b></p> <p>_____ permanent</p> <p>_____ temporary</p> <p><b>Use:</b></p> <p>_____ calibration</p> <p>_____ alignment</p>	<p><b>Hazardous Materials</b></p> <p>_____ cyanide plating materials</p> <p>_____ scintillation oil (from)</p> <p>_____ PCBs</p> <p>_____ methane</p> <p>_____ TMAE</p> <p>_____ TEA</p> <p>_____ photographic developers</p> <p>_____ other (list below)</p> <p>_____</p> <p>_____</p>	<p><b>General:</b></p> <p><b>Experiment Class:</b></p> <p>_____ Base Equipment</p> <p>_____ Temp. Mod. to Base Equip.</p> <p>_____ Permanent Mod. to Base Equipment</p> <p>_____ Major New Apparatus</p> <p><b>Other:</b> _____</p> <p>_____</p>

# LAB RESOURCES REQUIREMENTS LIST

CEBAF Proposal No.: \_\_\_\_\_  
(For CEBAF User Liaison Office use only.)

Date: \_\_\_\_\_

List below significant resources — both equipment and human — that you are requesting *from CEBAF* in support of mounting and executing the proposed experiment. Do not include items that will be routinely supplied to all running experiments, such as the base equipment for the hall and technical support for routine operation, installation, and maintenance.

**Major Installations** (either your equip. or new equip. requested from CEBAF)

---

---

---

---

---

---

---

---

---

---

New Support Structures: \_\_\_\_\_  
\_\_\_\_\_  
\_\_\_\_\_

**Data Acquisition/Reduction**

Computing Resources: \_\_\_\_\_  
\_\_\_\_\_  
\_\_\_\_\_

New Software: \_\_\_\_\_  
\_\_\_\_\_  
\_\_\_\_\_

**Major Equipment**

Magnets \_\_\_\_\_  
\_\_\_\_\_

Power Supplies \_\_\_\_\_  
\_\_\_\_\_

Targets \_\_\_\_\_  
\_\_\_\_\_

Detectors \_\_\_\_\_  
\_\_\_\_\_

Electronics \_\_\_\_\_  
\_\_\_\_\_

Computer Hardware \_\_\_\_\_  
\_\_\_\_\_

Other \_\_\_\_\_  
\_\_\_\_\_

**Other**

---

---

---

---

---

## CEBAF EXPERIMENTAL MAJOR REQUIREMENTS

Beam Time (Days)	27
Beam Energies (GeV)	2.4, 3.2, 3.5, 4.0
Beam Type	Unpolarized
Beam Current	$\leq 60 \mu\text{A}$
Targets Types	LD <sub>2</sub> , LH <sub>2</sub>
Power Deposition	< 50 watts

### BEAM TIME REQUEST

	<u>TIME (DAYS)</u>
Data Acquisition	21.7
Setup and Checkout	1.0
Angle Changes	0.8
Normalization Studies	1.5
Energy Changes	2.0
<b>TOTAL</b>	<b>27.0</b>

### SPECTROMETER REQUIREMENTS

	Electron Arm	Hadron Arm
Solid Angle	5 msr	4 msr
Momentum Acceptance	20%	40%
Momentum Resolution	$\leq 10^{-3}$	$\leq 10^{-3}$
Min Scattering Angle	14.5°	13.4°
Max Scattering Angle	61.4°	23.6°
Min Central Momentum	0.7 GeV/c	0.9 GeV/c
Max Central Momentum	2.4 GeV/c	1.7 GeV/c
Particle ID Required	$\pi^-/e^-$	$\pi^+/K^+$ , $p/K^+$
Required Ratio	0.01	0.005

**Longitudinal and Transverse Cross Sections in the  $d(e,e'K^+)YN$   
Reactions at  $Q^2 = 0.5$  to  $2$  (GeV/c)<sup>2</sup>**

**A. Abokor, Shelton Beedoe (Spokesman), S. Danagoulian, C. R. Jackson,  
S. Mtingwa**

*Physics Department, North Carolina A & T State University*

**O. K. Baker\* (Co-spokesman), K. Beard, W. W. Buck\*, T. Eden, R. Madey†,  
K. M. Maung, L. Tang\*, R. A. Williams**

*Physics Department, Hampton University*

*\* and jointly, Physics Division, CEBAF*

*† and Department of Physics, Kent State University*

**C. C. Chang, P. Markowitz (Co-spokesman)**

*Department of Physics and Astronomy, University of Maryland*

**D. Abbott, R. Carlini, Y. Chen, R. Ent, D. Mack, S. Majewski, J. Mitchell,  
W. Vulcan, S. Wood**

*Physics Division, CEBAF*

**B. Zeidman**

*Physics Division, Argonne National Laboratory*

**E. Hungerford, K. Lan, B. Mayes**

*Physics Department, University of Houston*

**J. Napolitano**

*Department of Physics, Rensselaer Polytechnic Institute*

**T. Angelescu, A. Mihul**

*Bucharest University, Bucharest, Romania*

**F. Garibaldi, M. Iodice, S. Frullani, E. Cisbani, G. M. Urciuoli, R. De Leo,  
G. Lolos, R. Perrino, T. Leone**

*INFN, Rome*

**Ts. Amatuni, H. Mkrтчyan, V. Tadevosian**

*Yerevan Physics Institute, Yerevan 375036, Armenia*

## Abstract

In the one-photon exchange approximation the cross section for the electroproduction reaction  $d(e, e'K^+)YN$ , where  $Y$  is either  $\Lambda$ ,  $\Sigma^0$  or  $\Sigma^-$  and  $N$  is a neutron or proton, is a function of four response functions when both target and incident beam are unpolarized. The experiment will do detailed separation of the transverse and longitudinal response functions and ascertain modifications of these response functions for the proton that result from interactions in a nuclear system. The particular virtue of the experiment is that the deuteron is the simplest nucleus in which to study the effects of the  $\Lambda$ -n final state interactions on the separate L and T response functions and modifications to the elementary amplitudes for the isolated proton. Moreover, the experiment shall provide much needed data for the determination of the elementary  $n(e, e'K^+)\Sigma^-$  amplitudes for the neutron. These results will form the basis for a systematic study to be extended to heavier nuclei and higher energies. The kinematic range for this experiment will cover the electron squared four-momentum transfer from 0.5 to 2  $(\text{GeV}/c)^2$ . The High-Momentum Spectrometer (HMS) and Short-Orbit Spectrometer (SOS) in Hall C will be used to measure the scattered electron and hadron momenta, respectively.

# 1. Introduction

The understanding of hadronic structure is one of fundamental importance in nuclear and high energy physics. One of the frontier areas of experimental intermediate-energy nuclear physics research is the study of nucleons and nuclear systems with strangeness degrees of freedom. Kaon electroproduction is one example of such a study. Measuring the elementary amplitudes for  $K^+$  electroproduction on the neutron will provide data on hadronic coupling; furthermore, by studying strange meson production from the bound nucleon (i.e., proton), one can in principle deduce modifications to the strange quark production.

In general, QCD has been successful as a theory that describes the strong interactions. At high energies and at large momentum transfers (deep inelastic scattering region), asymptotic freedom allows the application of perturbation theory to describe the structure and interactions of hadrons. At CEBAF energies, one probes the so called transition region from the non-perturbative confinement region to the region of asymptotic freedom. Here, phenomenological models describe the strong hadronic interactions because the non-perturbative region of QCD is not well understood. The electromagnetic properties of hadrons (strong coupling constants, transition magnetic moments) can further serve to illuminate models for describing the strong interaction<sup>1, 2, 3</sup>.

# 2. Motivation

Past experimental work in electromagnetic production of strangeness on heavy nuclear systems (where heavy means nuclear mass  $\geq 2$ ) has mostly concentrated on looking for bound hypernuclear states<sup>4, 5, 6</sup>. Existing kaon electroproduction experiments planned at CEBAF will be done at low  $Q^2$  values,  $Q^2 = 0$  [7] and  $Q^2 = 0.2$  (GeV/c)<sup>2</sup> [8]. In contrast, this proposal will extend the range of  $Q^2$  to  $0.5 \leq Q^2 \leq 2$  (GeV/c)<sup>2</sup> and determine the elementary  $n(e, e'K^+)\Sigma^-$  amplitudes for the neutron as well as study the modifications of the elementary

$p(e, e'K^+)\Lambda$  amplitudes for a weakly bound proton. In this multinucleon system, a longitudinal and transverse (L/T) separation will be done to ascertain the L & T responses in kaon electroproduction modified by the presence of another nucleon. Therefore, this experiment will address the following physics issues at high  $Q^2$ :

- i) study the  $\Lambda n$  final state interactions in the separated L/T channels,
- ii) determine the elementary neutron amplitudes and
- iii) attempt to establish data for  $n(e, e'K^+)$  in the separated L/T channels.

The proposed experiment will perform detailed separations of the transverse and longitudinal response functions,  $\sigma_U$  and  $\sigma_L$ , first on the  $\Lambda$  (and second on the  $\Sigma^- + \Sigma^0$ ), in the reaction



where  $Y$  is either a  $\Lambda$ ,  $\Sigma^0$  or  $\Sigma^-$  hyperon and  $N$  is the associated spectator nucleon. With

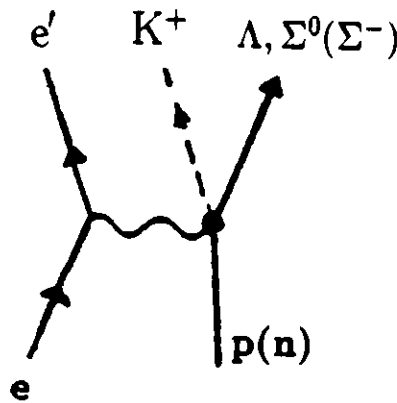


Figure 2.1: **Feynman diagram for the electroproduction reaction  $d(e, e'K^+)YN$ , where  $Y$  is either  $\Lambda$ ,  $\Sigma^0$  or  $\Sigma^-$ . Assuming one-photon exchange approximation this is written as  $\gamma_\nu + d \rightarrow K^+ + \Lambda, \Sigma$ .**

the deuteron target, the reaction (2.1), depicted in Fig. 2.1, can be decoupled into either one of the three possible reactions as



where the scattered electron and the electroproduced kaon will be detected in coincidence in the final state.

For electroproduction on the deuteron system, one is able to experimentally separate the  $\Lambda$  and  $\Sigma$  hyperons (by missing mass) assuming that the neutron or proton spectator in the final state has very small initial and final kinetic energies. Only the proton can contribute to  $\Lambda$  final states, allowing a clean comparison of the yield from deuterium and the yield from hydrogen. Previous works indicate that the  $K^+$ -n interaction should be small compared to the nucleon-hyperon interaction<sup>4</sup>. Then, in principle, the  $\Lambda$ -n interaction can be isolated.

Theoretical calculations using purely transverse photon ( $Q^2 = 0$ ), show a large effect due to the inclusion of  $\Lambda n$  final state interaction in the calculation<sup>9</sup>. The result of the calculation, shown in Fig. 2.2, also indicates the effects due to different partial waves. Such calculations predict different behavior in the longitudinal channel because the longitudinal virtual photon couples differently. In Fig. 2.3, a prediction of the sensitivity of the inclusive cross section, plotted vs  $\theta_K$ , to the  $\Lambda n$  final state interaction is shown<sup>10, 11</sup>. This means that even for the unseparated cross section, one should, with  $< 5\%$  measurement, be able to observe uncertainties in the cross section due to the  $\Lambda n$  final state interaction, but with less sensitivity. Since final state interactions (FSI) are expected to differ in the L & T channels, the separated response functions can provide additional insights.

Another physics issue that this experiment will address is the region around the  $\Sigma N$  threshold, referred to as the cusp region. In this region there is a rise in the cross section due to an interference with the  $\Sigma N$  channel. Figure 2.4 shows the theoretical inclusive cross section vs missing mass for a  $d(e, e'K^+)\Lambda n$  reaction. The bottom figure depicts the expanded cusp region, about 5 MeV in width, where the contributions from different partial waves are seen to be dominated by s wave triplet<sup>12</sup>. Hence the separated response functions in the  $\gamma^* + d$  reaction are ideal tools to study this region since the virtual photon can excite these spin states.

Presently there are no quality data for  $K^+$  electroproduction from the neutron. The only data<sup>13, 14</sup> are from the inclusive  $d(\gamma, K^+)X$  reaction<sup>15</sup>; previously approved CEBAF experiments will be done at low  $Q^2$ . Because the deuteron is the simplest practical neutron source, this experiment will provide data for the neutron amplitudes. Model calculations ascribe a larger cross section for the  $n(e, e'K^+)\Sigma^-$  reaction in comparison with the  $p(e, e'K^+)\Sigma^0$  reaction<sup>16</sup>. This and the availability of the proton data will facilitate obtaining the neutron amplitudes.

The neutron amplitudes will be determined by subtracting out the proton contribution (separately determined by E93-018) measured at the same kinematics and with the same

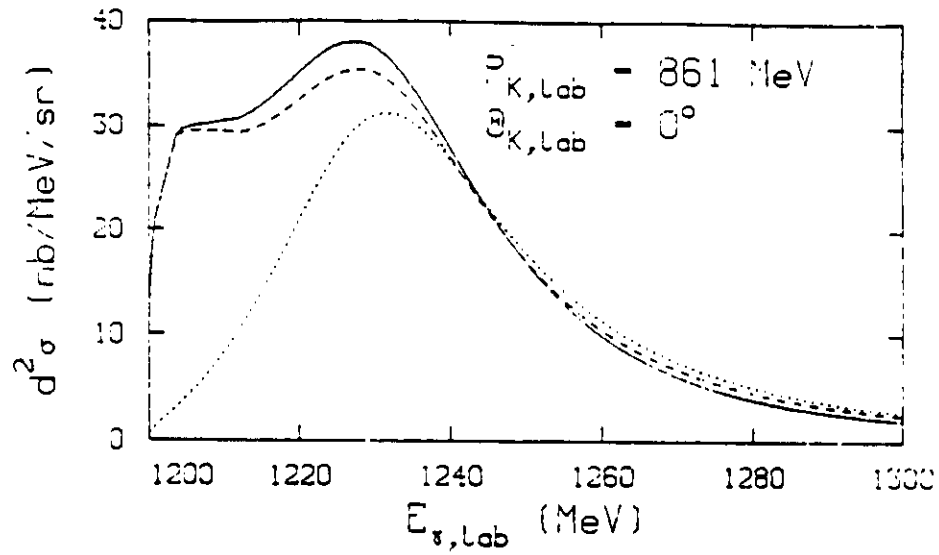


Figure 2.2: Comparison of  $d^2\sigma = \frac{d^2\sigma}{dP_K d\Omega_K}$  without (dotted line) and with  $\Lambda n$  interaction ( $l = 0$ , dashed line;  $l = 0-3$ , solid line) using real photons with  $Q^2 = 0$ [9].

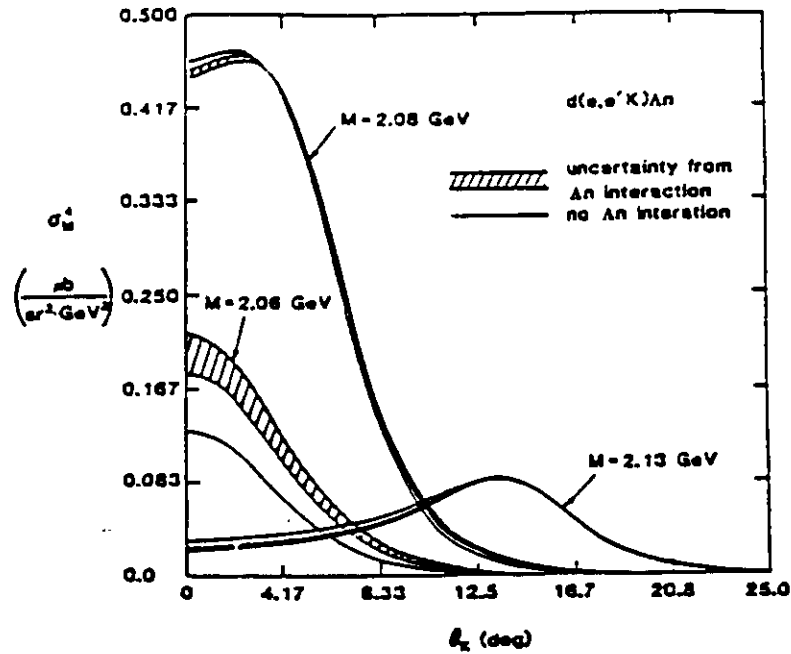


Figure 2.3: Calculation showing sensitivity of the inclusive cross section to the  $\Lambda n$  final state interaction plotted vs  $\theta_K$  in the lab[10].

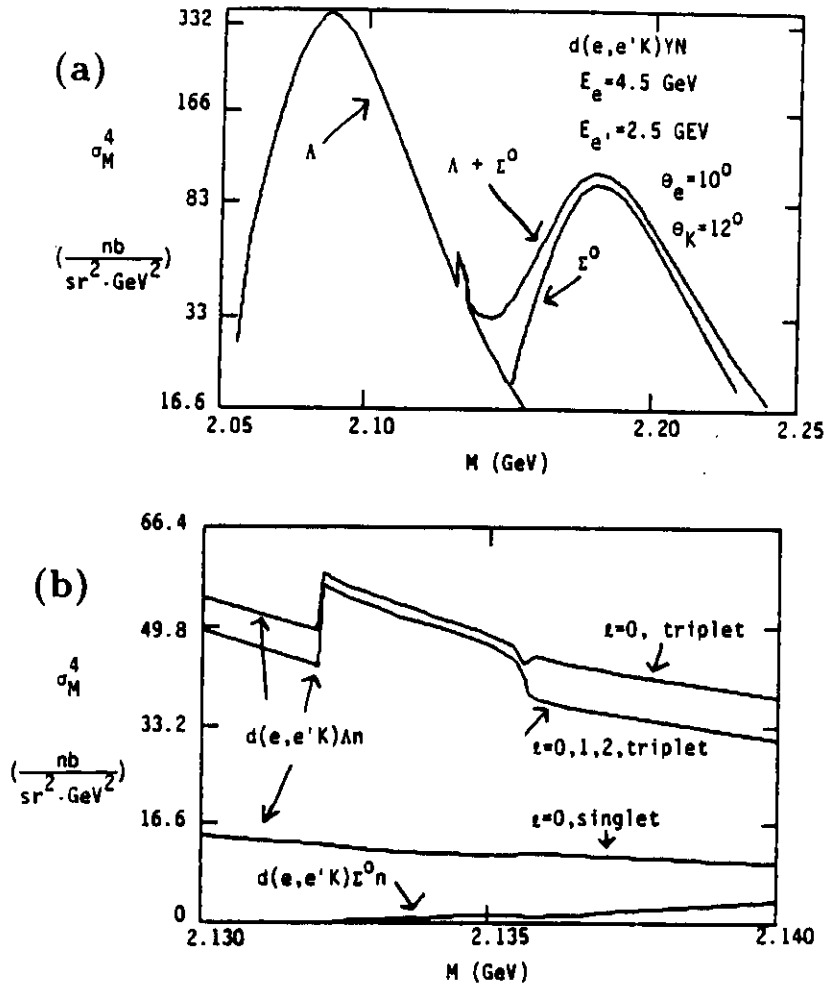


Figure 2.4: Theoretical calculation of the inclusive cross section for the  $d(e, e'K^+)\Lambda n$  reaction. The region around the  $\Sigma N$  threshold called the cusp region, exhibits an enhancement in the total cross section. (b) Expanded cusp region with different partial waves contributions[12].

detectors. Naively, the ratio of the  $\Lambda$  to  $\Sigma^0$  contributions will be fixed, and the  $\Sigma^-$  contribution determined by subtracting (from the combined  $\Sigma^0 + \Sigma^-$  yield) the  $\Lambda$  yield  $\times$  the ratio of  $\Sigma^0/\Lambda$ . More sophisticatedly, the measured yields on hydrogen can be input into a theoretical model, as well as the  $\Lambda$  and ( $\Sigma^0 + \Sigma^-$ ) yields from deuterium. The model can then be used to predict the  $\Sigma^-$  yield, allowing for different final state interactions between  $\Lambda$  and  $\Sigma$  channels.

By separately looking at the reaction in Eqs. 2.2 and 2.3 with longitudinal (virtual) photons compared to transverse (virtual) photons, one can hope to disentangle the electromagnetic vertices, just as in the case of a bare proton. If the electroproduced kaon is detected along the direction of the virtual photon (the forward or  $\mathbf{q}$  direction), then the associated hyperon must be collinear with that kaon from simple momentum conservation (if the relative p-n momentum is small in the initial deuteron), additionally, angular momentum conservation selects specific multipole transitions corresponding to the relative K-Y partial waves, i.e., there is a mapping from multipole amplitudes to partial wave amplitudes.

## 2.1 Theoretical overview of meson electroproduction

The reaction

$$e + A \rightarrow e' + K^+ + Y + (A - 1) \quad (2.5)$$

forms the basic reaction for kaon electroproduction off a nuclear target. In the above reaction  $Y$  is either a  $\Lambda$ ,  $\Sigma^0$  or  $\Sigma^-$  hyperon and  $(A-1)$  represents the residual nucleus. For  $A = 1$  and assuming one-photon exchange, this can be written as

$$\begin{aligned} \gamma_v + p &\rightarrow K^+ + \Lambda, \Sigma^0 \\ \gamma_v + n &\rightarrow K^+ + \Sigma^- \end{aligned} \quad (2.6)$$

in which the exchanged virtual photon's mass is the squared four-momentum transfer to the target nucleon. Knowledge of the 4-momentum of the left hand side of Eq. (2.6) and 4-momentum of the  $K^+$  is sufficient to identify the residual baryon  $\Lambda$ ,  $\Sigma^0$  or  $\Sigma^-$  by its missing mass  $M_m$ , given by

$$M_m^2 = (e - e' + N - K)^2. \quad (2.7)$$

Other Lorentz invariant quantities for the kinematics are defined by

$$\begin{aligned} \gamma_v^2 &= (k - k')^2 = q^2 \\ s &= W^2 = (\gamma_v + N)^2 \end{aligned}$$

$$\begin{aligned}
-t &= (\gamma_\nu - K)^2 \\
Q^2 &= -q^2
\end{aligned}
\tag{2.8}$$

where the four momenta are  $k = (E, \mathbf{k})$ ,  $k' = (E', \mathbf{k}')$ ,  $K = (E_K, \mathbf{K})$  and  $q = (\nu, \mathbf{q})$  for the incident electron, scattered electron, ejected kaon and virtual photon respectively;  $N$  is the target nucleon four momentum,  $\nu = E - E'$  is the energy of the virtual photon, and  $W = \sqrt{s}$  is the total hadronic system mass. If the nucleon is bound within the nucleus, then it can be considered as a virtual (off mass-shell) nucleon and  $N^2 \neq M_N^2$ .

The kinematics variables and the reaction planes are shown in Fig. 2.5. The electronic

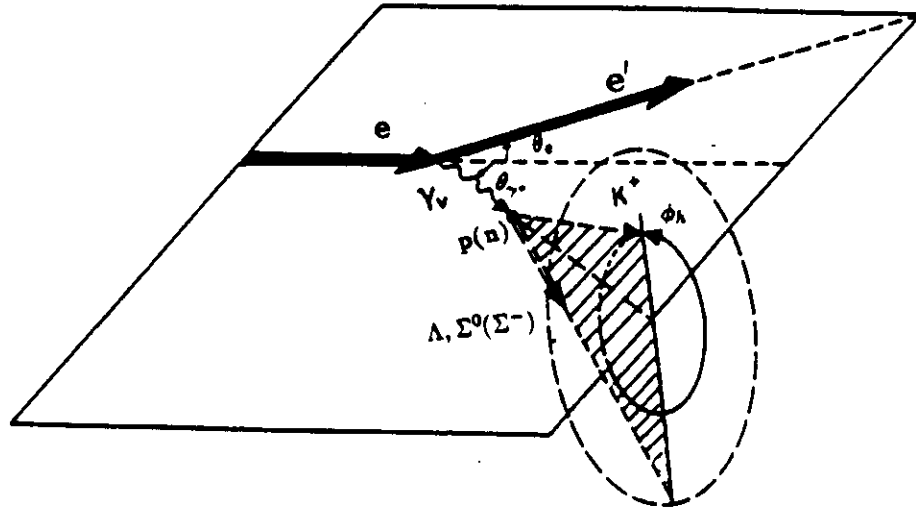


Figure 2.5: Definition of scattering planes for electrons (initial and final), and ejectiles (kaon and residual particles).

scattering plane is defined as the plane containing the incident and scattered electrons, with  $\theta_e$  denoting the angle between the electrons. The symbol  $\phi_h$  is the angle between the electron scattering plane and the ejectile plane, defined as the plane containing the ejected kaon and the associated  $\Lambda$  or  $\Sigma$  particle in the final state. These form a coordinate system in which the z-axis is the direction of the virtual photon, and  $\theta_K$  and  $\phi_h$  are the given spherical angles. The x- and y-axes are thus parallel and perpendicular to the electronic scattering plane.

The cross section for the reaction in Eq. (2.6) can be expressed as<sup>17, 18</sup>

$$\frac{d^4\sigma}{dQ^2 ds dt d\phi} = 2\pi \Gamma \frac{d^2\sigma}{dt d\phi}.
\tag{2.9}$$

The virtual photon flux  $\Gamma$  is given by

$$\Gamma = \frac{\alpha(s - M_N^2)}{(4\pi)^2 E^2 M_N^2 Q^2} \frac{1}{1 - \epsilon} \quad (2.10)$$

and

$$\frac{d^2\sigma}{dt d\phi} = \frac{d\sigma_U}{dt} + \epsilon \frac{d\sigma_L}{dt} + \epsilon \frac{d\sigma_P}{dt} \cos 2\phi + \sqrt{\frac{1}{2}\epsilon(\epsilon + 1)} \frac{d\sigma_I}{dt} \cos \phi \quad (2.11)$$

is the single hadron production cross section by virtual photons. The cross sections  $\sigma_U$  and  $\sigma_L$  are the components from photons with their electric vector perpendicular or parallel to the hadronic current 3-vector, i.e., transverse and longitudinal photons. The cross section  $\sigma_P$  represents the interference contributions from the transverse component of the virtual photon and  $\sigma_I$  is due to interference between the transverse and longitudinal components of the virtual photon. The parameter  $\epsilon$ , ( $0 \leq \epsilon \leq 1$ ), denotes the degree of polarization of the virtual photon. It is expressed in terms of incident and final electron kinematics as

$$\epsilon = \left[ 1 + 2 \left( 1 + \frac{\nu^2}{Q^2} \right) \tan^2(\theta_e/2) \right]^{-1}. \quad (2.12)$$

The separation of the four response functions would require measurement of the  $\epsilon$ - and  $\phi$ -dependence of the kaon electroproduction reaction. However the last two  $\phi$  dependent terms can be eliminated by a proper choice of spectrometer settings. By varying  $\epsilon$ , the remaining first two terms can be separated readily. The response functions in equation (2.11) are functions of  $(W^2, Q^2, t)$ .

## 3. Experimental Procedure

### 3.1 Separation of longitudinal and transverse response functions

The aim of this experiment is to perform a detailed study of the longitudinal and transverse response functions. The SOS (the hadron arm) will be placed such that, upon averaging, the  $\phi$ -dependent terms in Eq. 2.11 can be eliminated. We can then separate  $\sigma_U$  from  $\sigma_L$  by a Rosenbluth separation. Since only the sum of these response functions will be measured, by varying the polarization parameter  $\epsilon$ , the slope of the curve in Fig. 3.1 is a measure of the

longitudinal response function while the intercept, at  $\epsilon = 0$ , gives the transverse response function. The indicated uncertainties reflect only statistics, and we have used  $\sigma_U \sim \sigma_L$ .

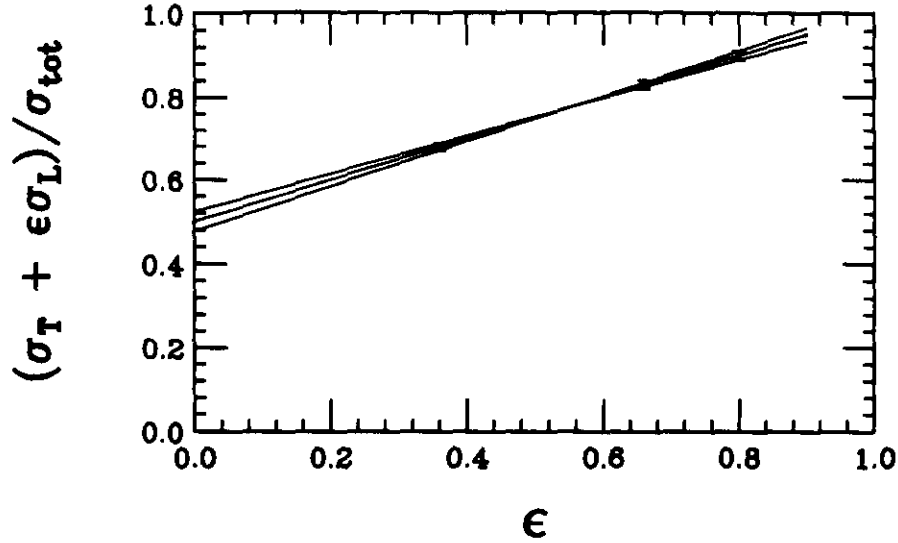


Figure 3.1: Rosenbluth separation of  $\sigma_U$  and  $\sigma_L$ . The indicated uncertainties are statistical only.

The kinematic settings for this experiment shall be the same as those already presented in experiment E-93-018, which does an L/T separation on a hydrogen target<sup>19</sup>. Because of the closeness of the  $\Sigma^0$  ( $M_{\Sigma^0}=1192$  MeV) and  $\Sigma^-$  ( $M_{\Sigma^-}=1197$  MeV) masses, this experiment will not be able to separate these hyperons when the missing mass is convoluted with the momentum distribution or Fermi smearing. Thus the experiment will utilize data from the  $p(e,eK^+)\Sigma^0$  reaction taken at the same kinematics, with the same detectors and acceptances to perform a subtraction. The quantity  $\sigma_D[K^+\Sigma^0 + K^+\Sigma^-] - \sigma_P[K^+\Sigma^0]$  measures the strange kaon meson production cross section from the neutron, ignoring the Fermi motion. It is crucial that the proton data be taken with the same experimental resolution, PID system, acceptances and detectors to minimize the systematic uncertainty in the subtraction of the  $K^+\Sigma^0$  final state from the combined  $[K^+\Sigma^- + K^+\Sigma^0]$ .

### 3.2 Longitudinal cross section

In the t-channel the virtual photon directly couples to the kaon. Only longitudinally polarized photons will scatter in the forward direction from the kaon (or mesonic current of the nucleon) in the t-channel; and the kaon form factor is thus extracted from the longitudinal component.

The  $t$ -channel contribution is enhanced when the variable  $|t|$  is at a minimum, which depends on the squared virtual photon mass as shown in Fig. 3.2. Pion electroproduction data show

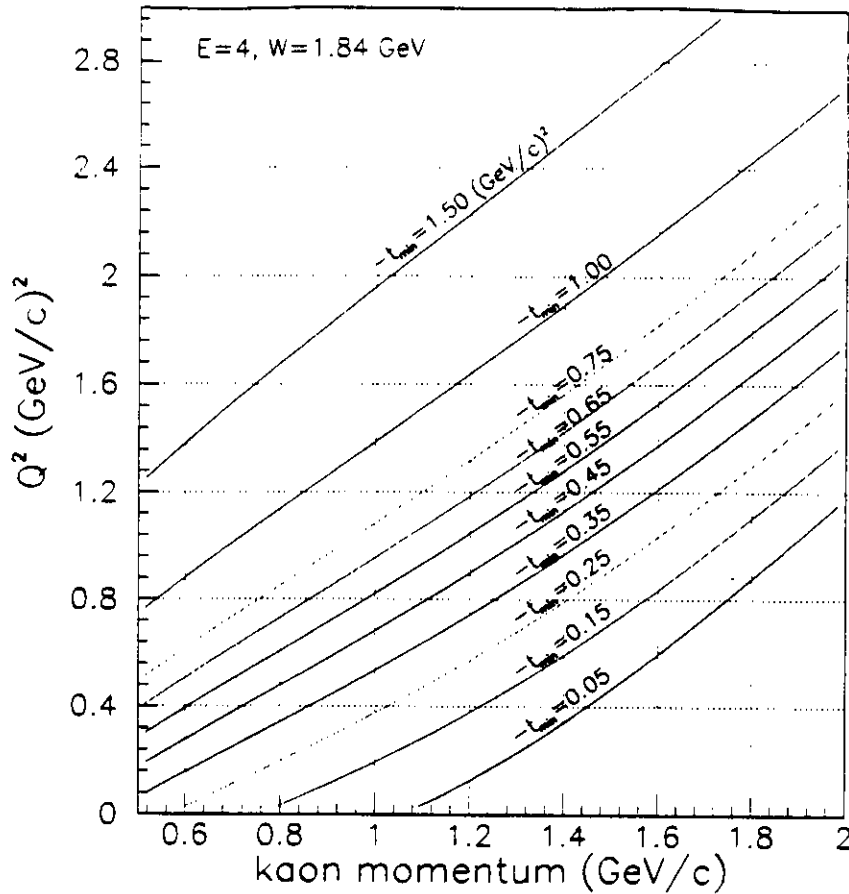


Figure 3.2: The variable  $t_{\min}$  dependence on  $(Q^2, p_K)$ ,  $p_K =$  kaon momentum. This experiment will cover  $0.8 \leq p_K \leq 1.8$  (GeV/c) and  $0.5 \leq Q^2 \leq 2$  (GeV/c) $^2$ .

a decreasing dependence of  $\sigma_L$  on  $|t|^{20}$ . This is expected for kaon electroproduction as well, where  $\sigma_L$  dominates at low  $t$  over the remaining three cross sections. In Fig. 2.1 the virtual photon couples to a virtual kaon emitted by the target nucleon. Most of the physics discussed here will seek to separate out the  $t$ -channel  $K^+$  production mechanism from the other possibilities because this is the relevant mode which involves the kaon electromagnetic form factor—it is the Born term in the  $t$ -channel. Replacing  $p$  by  $n$ , and replacing  $\Lambda$  and  $\Sigma^0$  by  $\Sigma^-$ , will give similar diagrams for the neutron.

One can study the  $t$ -dependence of the  $d(e, e'K^+)\Lambda n$  electroproduction process to isolate the  $t$ -channel exchange contribution in the longitudinal response function in the deuteron system, similar to the study on the bare proton<sup>19</sup>. Because the reaction shown in equation

(2.1) should be independent of whether the reaction takes place on a nucleon or in a nucleus (if the spectator approximation is valid), one expects the ratio of the longitudinal response functions in  $\Lambda$  production,  $\sigma_L^D(Q^2)/\sigma_L^P(Q^2)$ , to be unity at all values of the momentum transfer squared (after correcting for the Fermi motion). Any deviations from this result would signal a modification of the response function due to either the nuclear binding (an off-shell effect) or the  $\Lambda$ -n FSI. The virtue of the deuteron target is that it provides the simplest nucleus for studying differences with respect to elementary electroproduction.

Figure 3.3 (left) shows the theoretical prediction of the unseparated inclusive cross section for the  $d(e, e'K^+)\Lambda n$  reaction plotted against kaon angles. For different kaon form factor, governed by vector meson mass, about 5% sensitivity level is observed in the combined cross section. The calculation also distinguishes the different types of potentials<sup>11, 21, 22</sup>. However, calculations for  $p(e, e'K^+)\Lambda$ , Fig. 3.3 (right), shows a remarkable large sensitivity to the kaon form factor in the longitudinal channel compared to the transverse channel<sup>23</sup>. One can conclude that small effects in the transverse channel may be larger in the longitudinal channel; and effects that are unnoticeable or small in the combined cross section are amplified in the separated cross sections.

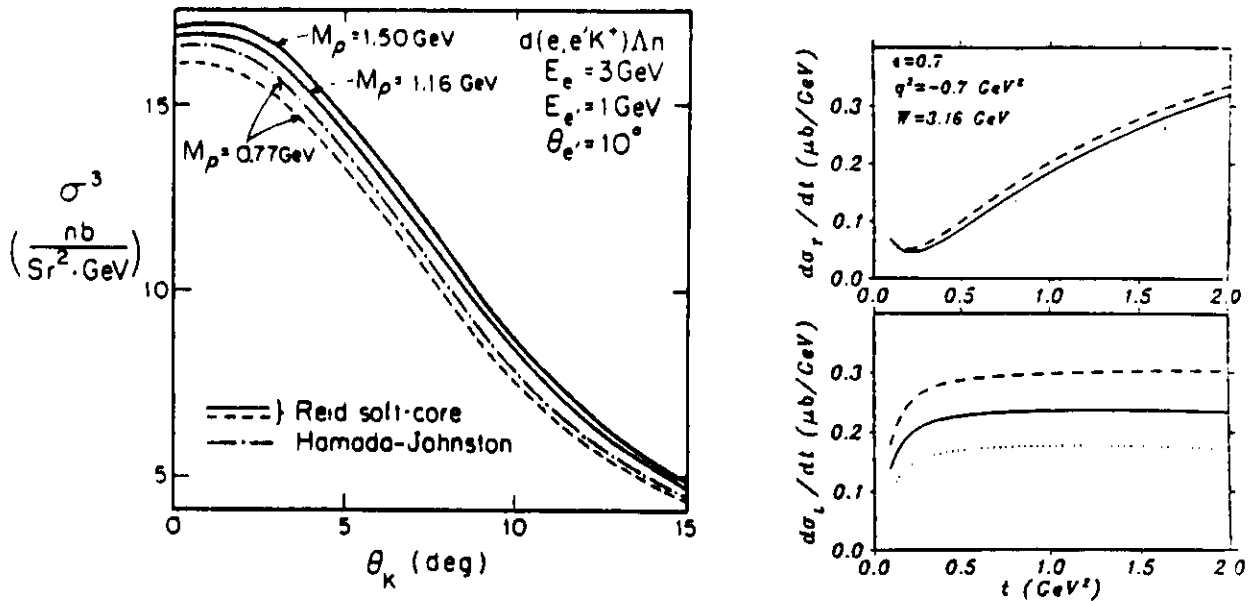


Figure 3.3: **Theoretical calculation showing weak sensitivity to kaon electromagnetic form factor for the combined cross section (left) in  $d(e, e'K^+)\Lambda n$ . Utilizing  $p(e, e'K^+)\Lambda$  reaction, a mild sensitivity shows up in transverse cross section (right top) and a much larger sensitivity in longitudinal (right bottom) cross section[23].**

### 3.3 Transverse cross section

The electroproduction of pseudoscalar mesons by transversely polarized virtual photons has been examined in a naive quark-parton model<sup>24</sup>. The model predicts that the ratio of the transverse cross section for  $K^+\Sigma^0$  production on the proton to  $K^+\Sigma^-$  production on the neutron is 1:2 reflecting the probability of finding the  $ud$  quarks in the proton in an  $I=1$  state compared to the probability of finding the  $dd$  quarks in the neutron in an  $I=1$  state<sup>24</sup>. The important point is that it is necessary to do an L/T separation to see the behavior of  $\sigma_U$ , the transverse part of the cross section.

There is also a perturbative QCD (pQCD) prediction<sup>25</sup> for photoproduction of kaons. The calculation is the leading twist, Born approximation helicity amplitudes for s-channel scattering from valence quarks. Shown in Fig. 3.4, the cross section is plotted as a function

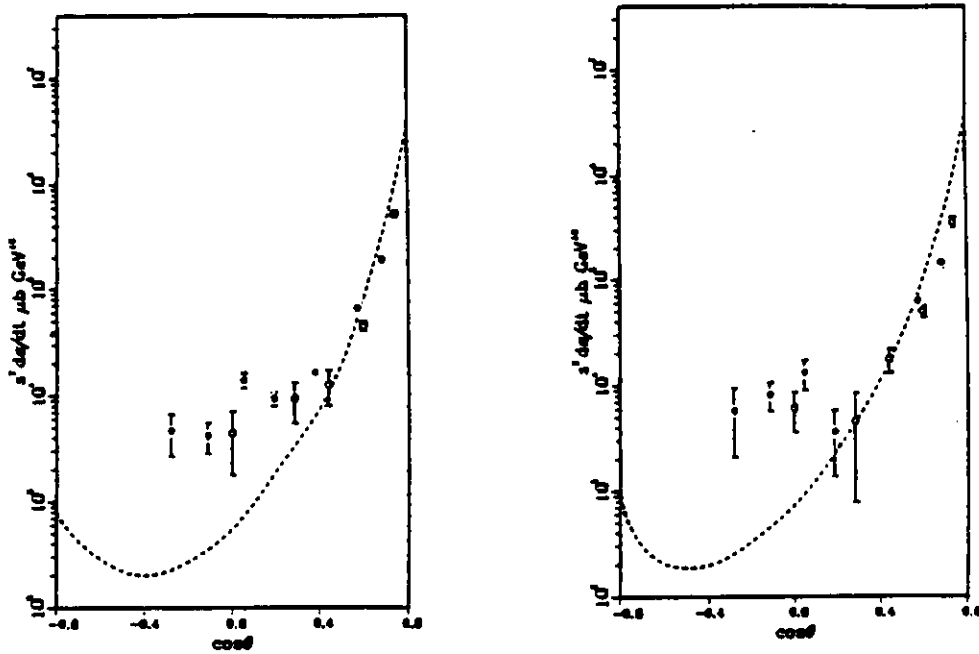


Figure 3.4: Unpolarized cross section  $s^7 d^2\sigma/dt^2$  with  $\epsilon=0.01$ , for  $\gamma p \rightarrow K^+\Lambda^0$  (left) and  $\gamma p \rightarrow K^+\Sigma^0$  (right)[25] compared to the data[26] for 4 (6) GeV, solid (open) circle.

of  $\cos \theta$ , where  $\theta$  is the angle between the photon and the outgoing kaon (this is equivalent to  $t$ ). The calculation is sensitive to the quark wave functions, which give a different behavior for the  $\Lambda$  channel versus the  $\Sigma$  channel (the minimum for the  $\Lambda$  occurs around  $\cos \theta = -0.4$ , while the dip for the  $\Sigma$  occurs around  $\cos \theta = -0.5$ ). As can be seen, the photoproduction data are not in perfect agreement with the calculation. At forward angles, the t-channel

contributes, while at backward angles the u-channel contributes. This prediction should hold more rigorously for the transverse part of the electroproduction cross section<sup>27, 28</sup>. For this experiment,  $0.2 \leq x_{Bj} \leq 0.5$  allows one to scatter predominantly from a valence quark, the L/T separation allows one to minimize the t-channel contribution, and the t-behavior will be mapped out by changing the kaon angle while keeping the electron arm fixed.

## 4. Experimental Conditions

### 4.1 Experimental arrangements and kinematics

The data on the deuteron target will be obtained with the apparatus in Hall C at CEBAF, namely, the High Momentum Spectrometer (HMS) and the Short Orbit Spectrometer (SOS). A plan view of Hall C is shown in Fig. 4.1. The momentum of the final scattered electron

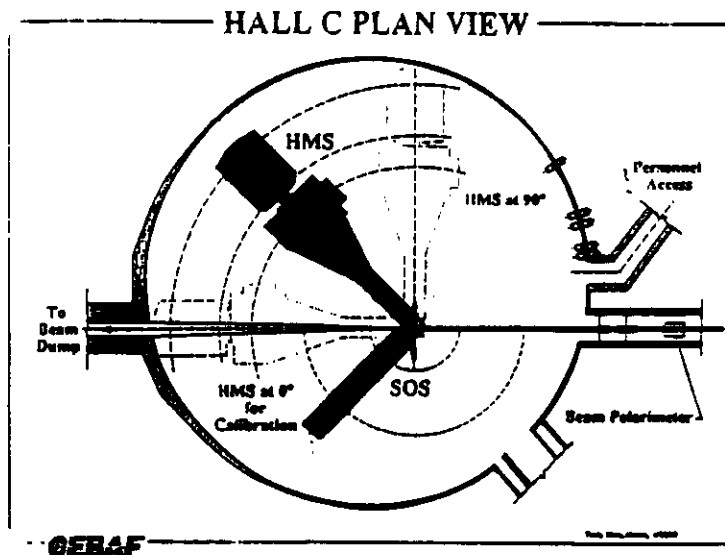


Figure 4.1: Set up of experimental Hall C. The scattered electrons will be detected in the HMS while the kaons will be detected in the SOS.

is measured by utilizing the HMS and the produced meson is observed in the SOS. For the

HMS arm, the detector stack follows three quadrupole magnets and one dipole magnet. A similar detector stack for the SOS arm is placed after one quadrupole magnet followed by two dipole magnets bending in opposite directions. The proposed detector stacks for the two spectrometers are shown in Fig. 4.2.

The choice of kinematics dictates the spectrometer settings listed in Table 4.1. The total c.m. energy  $W = \sqrt{s}$  is chosen here to be above the resonance region. Contours for these kinematic variables are shown in Fig. 4.3.

Table 4.1: Kinematics Settings

Kine.	$Q^2$	$E_e$	$E'_e$	$\theta_e$	$\theta_\gamma$	$W$	$\nu$	$\epsilon$	$x$
1a	0.50	2.40	0.80	29.56	13.04	1.84	1.60	0.54	0.17
1b	0.50	3.20	1.57	18.25	16.31	1.84	1.60	0.76	0.17
1c	0.50	4.00	2.39	13.16	18.10	1.84	1.60	0.86	0.17
2a	1.00	2.40	0.61	49.20	12.76	1.81	1.80	0.36	0.30
2b	1.00	3.20	1.38	27.69	18.08	1.81	1.80	0.66	0.30
2c	1.00	4.00	2.19	19.48	20.77	1.81	1.80	0.80	0.30
3a	1.50	2.40	0.61	61.37	12.98	1.69	1.85	0.28	0.43
3b	1.50	3.20	1.34	34.39	19.91	1.69	1.85	0.61	0.43
3c	1.50	2.40	2.23	23.42	23.56	1.69	1.85	0.78	0.43
4a	2.00	3.20	0.79	53.14	13.03	1.84	2.40	0.34	0.44
4b	2.00	3.50	1.09	42.51	15.33	1.84	2.40	0.46	0.44
4c	2.00	4.00	1.59	32.67	17.90	1.84	2.40	0.60	0.44

## 4.2 Uncertainties and background considerations

Fermi smearing of the missing mass will introduce uncertainty in the missing mass resolution. The magnitude of this, however, will not hamper the L/T separation or the separation of the  $\Lambda$  final states from the  $(\Sigma^0 + \Sigma^-)$  final states. Shown in Fig. 4.4 is a calculation of the cross section vs missing mass. It is seen that the  $\Lambda$  region is separated from the  $\Sigma$  region. Both regions are kinematically shifted when kaons are observed away from the direction of the virtual photon as seen in Fig. 4.4.

In the HMS arm, a gas Čerenkov will be used on-line to reject pions. Further pion discrimination will be achieved off-line by utilizing the lead-glass shower counter detector (see Fig. 4.5a). The hadron arm will utilize a time-of-flight (TOF) and an anti- $\pi$  coincidence

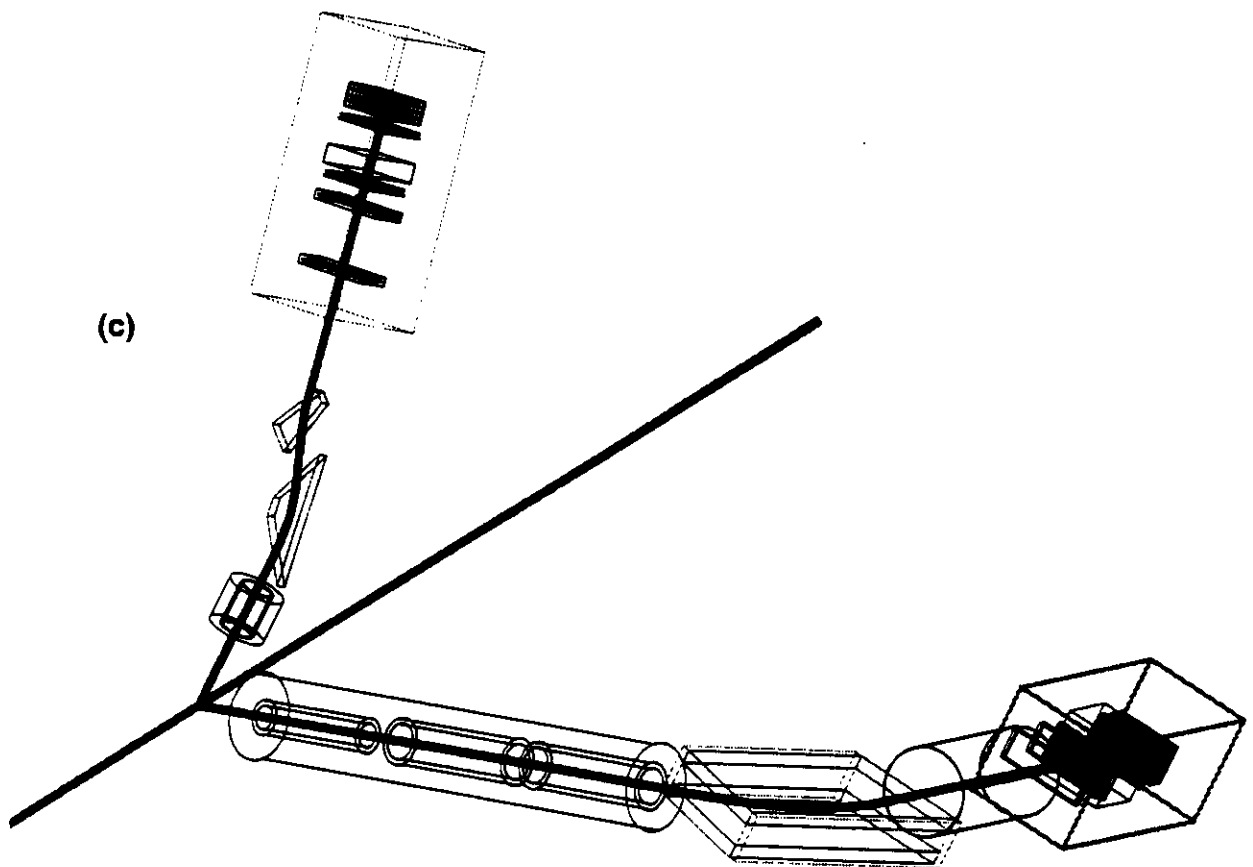
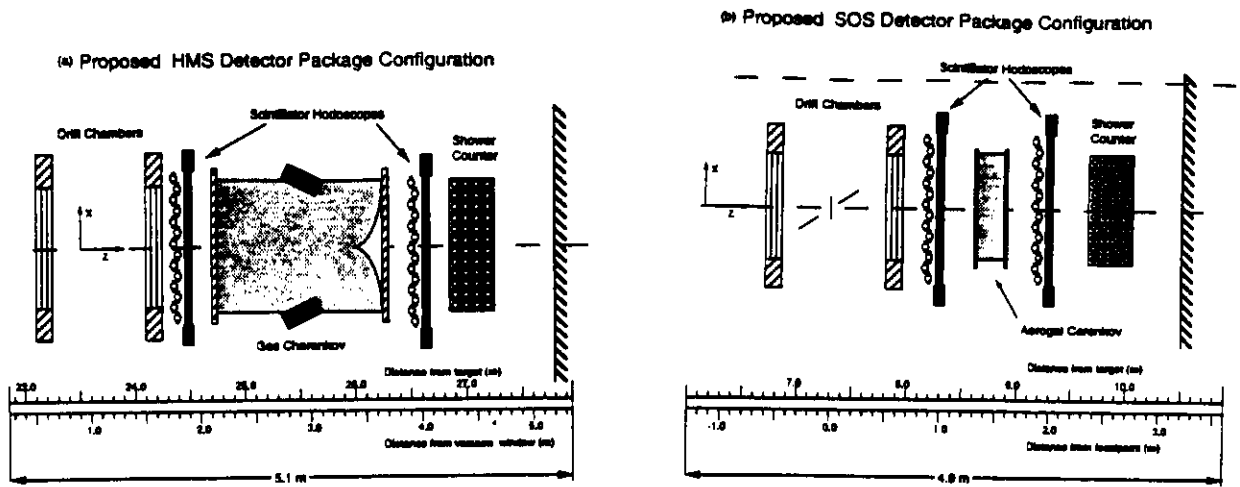


Figure 4.2: (a) HMS detector plan view. (b) SOS detectors plan view. (c) GEANT drawing of the two spectrometers at 45° from beam axis, SOS (left) HMS (right).

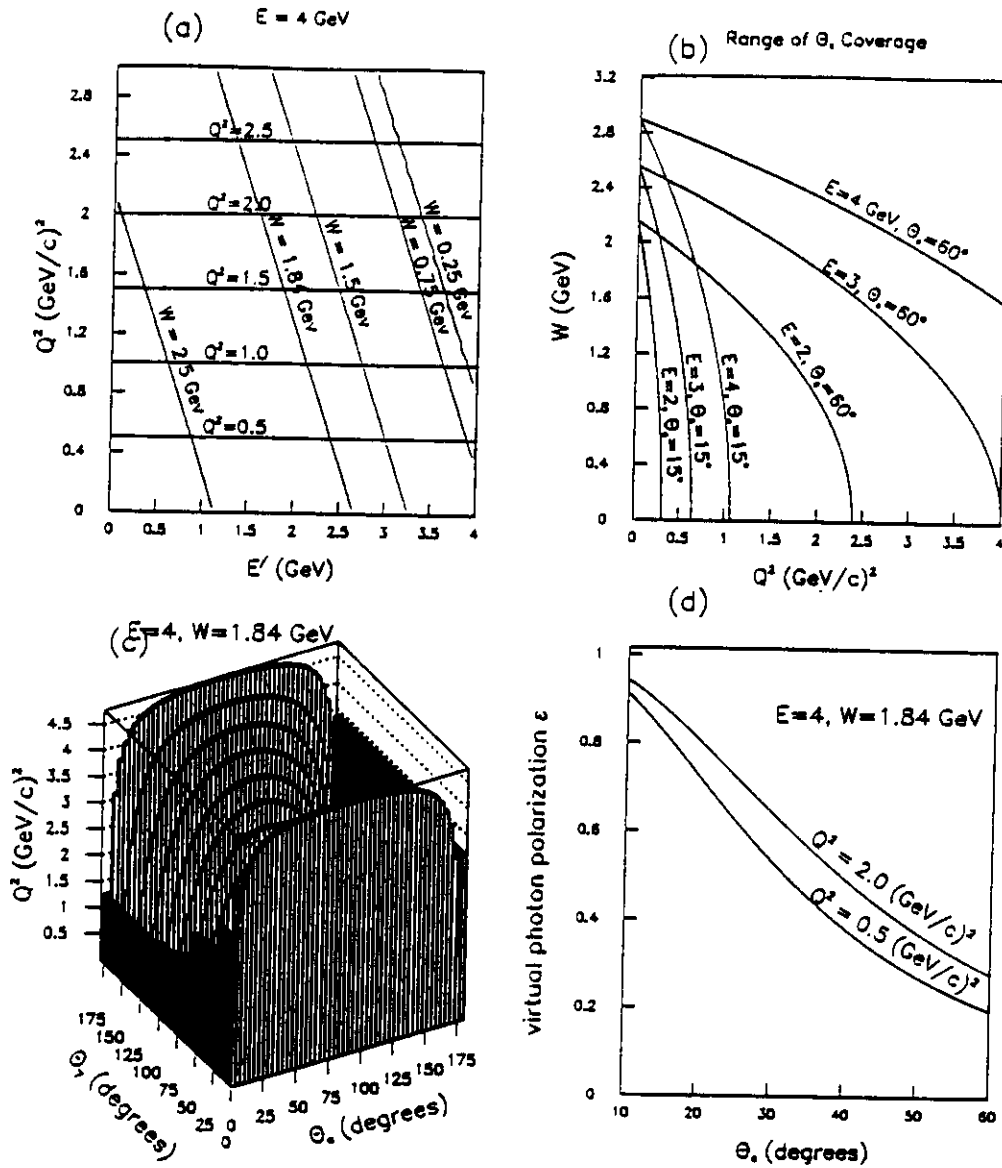


Figure 4.3: Kinematics contours describing available phase space. (a) The  $W$ -dependence in the  $(Q^2, E')$  plane. For this experiment,  $W$  will vary between 1.7 and 1.9 GeV. (b) Range of coverage for the electron arm in the  $(W, Q^2)$  plane. (c) Hypersurface for the dependence of  $Q^2$  on the scattered electron and virtual photon direction over possible combinations. (d) Virtual photon polarization parameter dependence on electron kinematics for the  $Q^2$  and  $W$  of this proposal.

$E=3 \text{ GeV}, E'=1.5 \text{ GeV}, \theta_e=12.5^\circ, \theta_{\gamma^*}=11.9^\circ, \theta_{K\gamma}=0, 6.5^\circ$

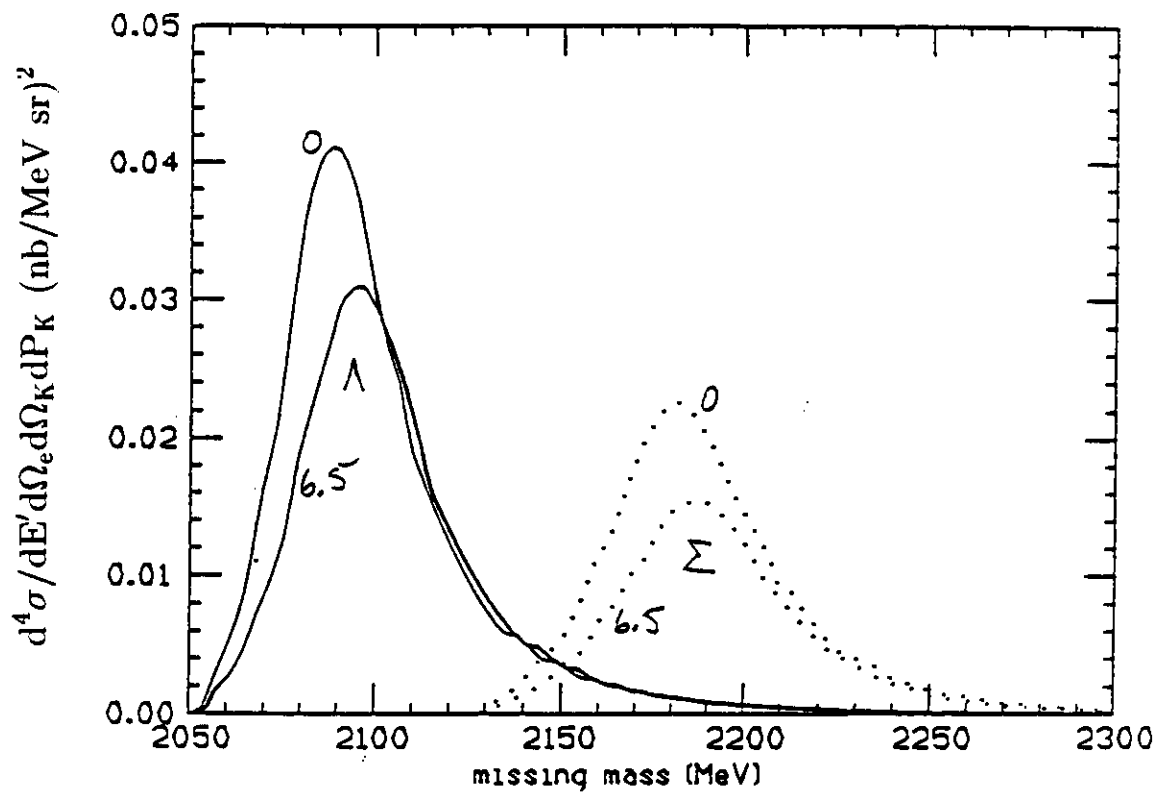


Figure 4.4: Smearing of the missing mass due to Fermi broadening[29].

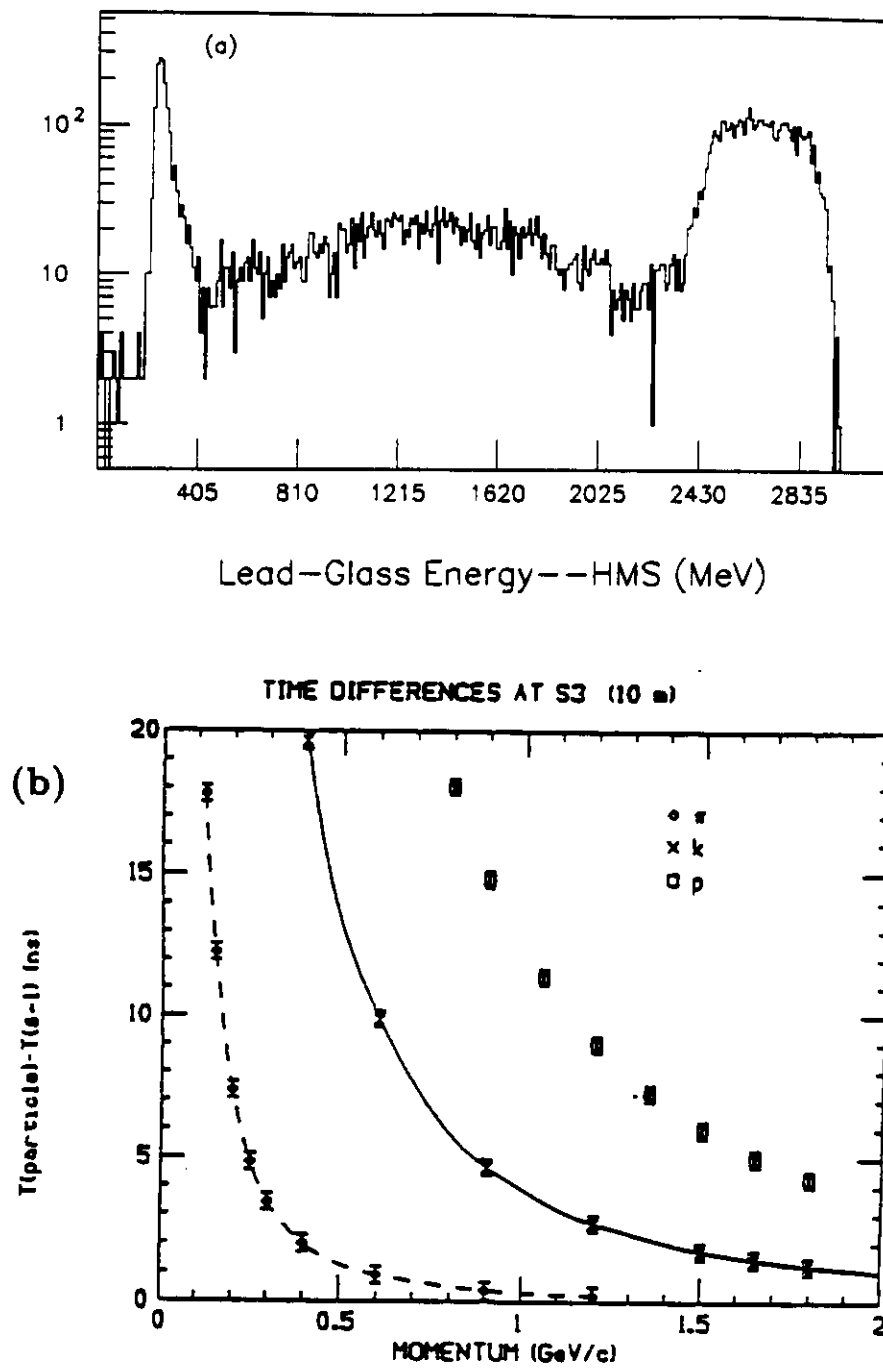


Figure 4.5: A GEANT simulated (a) electron-pion events, generated over a momentum range of  $3 \pm .25$  GeV/c in the HMS arm, and (b) TOF difference for  $\pi$ ,  $K^+$ , p separation in the SOS arm over a momentum range of 0.8 to 1.8 GeV/c.

mode trigger on-line to reject slow protons and pions. Off-line a TOF coincidence window on the order of  $\sim 1$  ns will further clean up the final kaon sample, as depicted in Fig. 4.5b.

### 4.2.1 Statistical uncertainty

At each kinematic point, the  $d(e, e'K)$  cross section will be measured with a statistical uncertainty of  $1\frac{1}{3}\%$ . For the range in  $\epsilon$  shown in Table 4.1, the statistical uncertainty resulting from the fit shown in Fig. 3.1 is  $\pm 5.8\%$  in the longitudinal response function while the uncertainty is  $\pm 3.4\%$  in the transverse response function.

Because the range in  $\epsilon$  is approximately the same for all  $Q^2$  values, the statistical uncertainty in the extracted response functions is also the same. The constraints on the neutron amplitudes and the longitudinal response function for kaon electroproduction in the neutron channel are slightly worse, since the uncertainty in the kaon form factor also enters. Additionally there is some theoretical uncertainty in the knowledge of the  $\Sigma$  modifications which come from our knowledge of the  $\Lambda$  modifications. The uncertainties from both the proton data and the deuteron data are added in quadrature to estimate the uncertainty in the neutron amplitudes. We estimate this uncertainty to be less than 8%.

### 4.2.2 Systematic uncertainty

In Eq. 2.11 the responses are functions of  $Q^2$ ,  $W$ , and  $t$ . The systematic uncertainties will thus be due to uncertainties in  $Q^2$ ,  $W$  and  $t$  (or the kaon angle). These in turn are due to the electron kinematics,  $E$ ,  $E'$  and  $\theta_{e'}$ , and kaon kinematics,  $P_K$  and  $\theta_K$ . We estimate the uncertainties in  $E$ ,  $E'$ ,  $\theta_{e'}$ ,  $P_K$  and  $\theta_K$  to be  $10^{-4}$ ,  $10^{-3}$ , 1.0 mr,  $10^{-3}$ , and 1.0 mr, respectively.

Table 4.2 lists the expected systematic uncertainties. As can be seen, the important systematics are the relative uncertainties between successive measurements. No uncertainty is assumed for how well the energy, angles, particle momenta and target thickness will translate between E93-018 and the present proposal. It is assumed that beam monitors, spectrometer tunes, and target cryogenics will be the same for the two experiments.

### 4.2.3 GEANT Monte Carlo

Both the HMS and SOS detectors have been simulated in GEANT<sup>30</sup>. With these simulations the systematics can be calculated—an effort that otherwise could cost a considerable amount of beam time. The simulation includes details of the detector geometry and material. The responses of the detector elements when particles propagate through the experimental set up are digitized and recoded into appropriate format consistent with the CODA data format.

Table 4.2: **Relative Uncertainties**

<b>Angle</b>	<b>0.5%</b>
<b>Target Density Variations</b>	<b>1.0%</b>
<b>Cell Walls</b>	<b>0.5%</b>
<b><math>K^+</math> absorbtion</b>	<b>1.0%</b>
<b>Detector Inefficiencies</b>	<b>1.0%</b>
<b>Kaon Decay</b>	<b>0.5%</b>
<b>Radiative Corrections</b>	<b>0.5%</b>
<b>Beam Current</b>	<b>1.0%</b>
<b>Acceptances</b>	<b>0.5%</b>
<b>Total Systematic</b>	<b>2.3%</b>

This allows one to develop and test tracking software and study detector resolution. Effects from processes like multiple scattering, particle decay, energy loss, etc. are calculated easily. The energy deposited in the 1-cm scintillator element for ( $\pi$ ,  $K^+$ , p) is shown in Fig. 4.6.

Magnetic fields are generated with TOSCA and used in the HMS arm to track particles through the system. These field maps are reasonable approximation of the magnetic elements. For a point-to-point tuning mode, Figs. 4.7a and b show the trajectories in the horizontal and vertical planes through the quadrupole and dipole magnets for the expected focussing (or defocussing). This is consistent with the RAYTRACE calculations[31]. The expected inelastic scattering off  $^{12}\text{C}$  is shown in Fig. 4.7c for a 2-GeV/c electron scattering at  $12^\circ$ . The peaks correspond to the ground (elastic scattering), first and second (inelastic scattering) excited states. These are, in this simulation, approximately separated by 5 MeV.

### 4.3 Count rate estimates

We estimate the rates in each detector using the luminosity set forth in the CEBAF Conceptual Design Report (CDR)<sup>32</sup>. The envisioned effective target length is 5 cm and beam currents of 20 to 60  $\mu\text{A}$ . Power dissipation in the target for this current should be minimal. In calculating the rates the laboratory cross section  $\frac{d^3\sigma}{dE'_e d\Omega_e d\Omega_K}$  was computed from experimental data (e.g. Refs. [13,33]) extrapolated for other  $Q^2$  and  $W$  values. For the singles rates, the eN cross section is written in the Rosenbluth form. The dipole form factor has been used to describe the momentum-transfer dependence. The cross section has been computed both for protons and neutrons and added incoherently, similar to that used in Ref. [34]. The kaon laboratory cross section was integrated over momentum bite of  $\pm 0.20p_0$ .

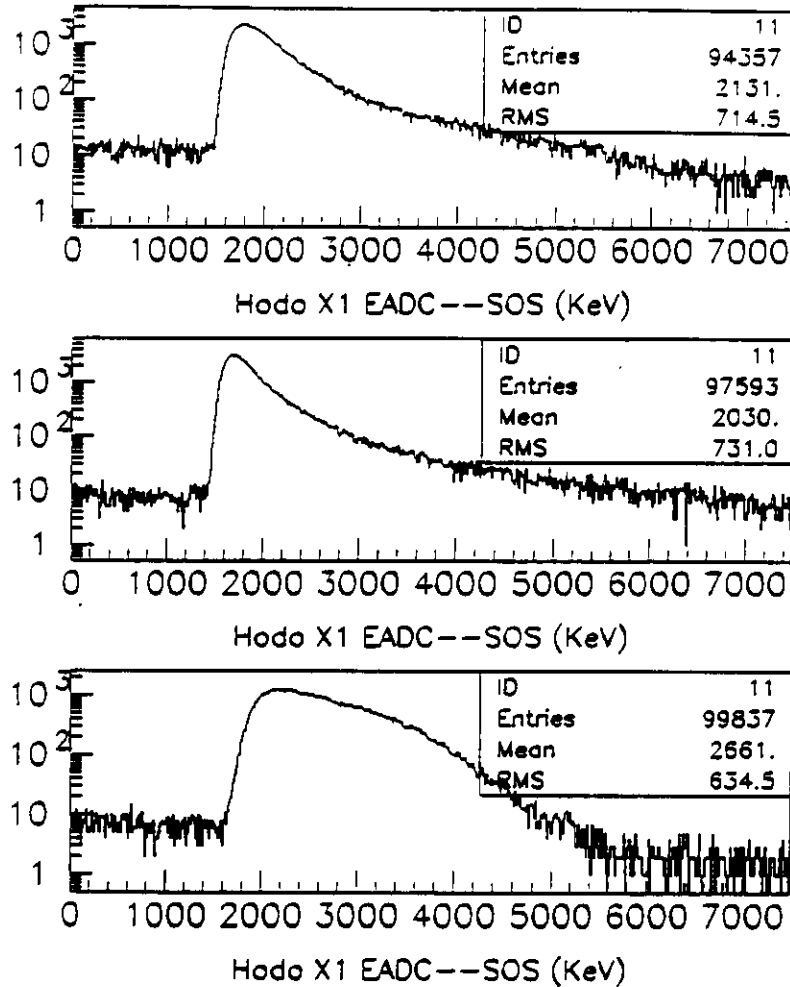


Figure 4.6: The energy deposited in the SOS X1 scintillator array for  $\pi$  (top),  $K^+$  (middle) and proton (bottom). The events were generated over a momentum range of 0.8–1.8 GeV/c.

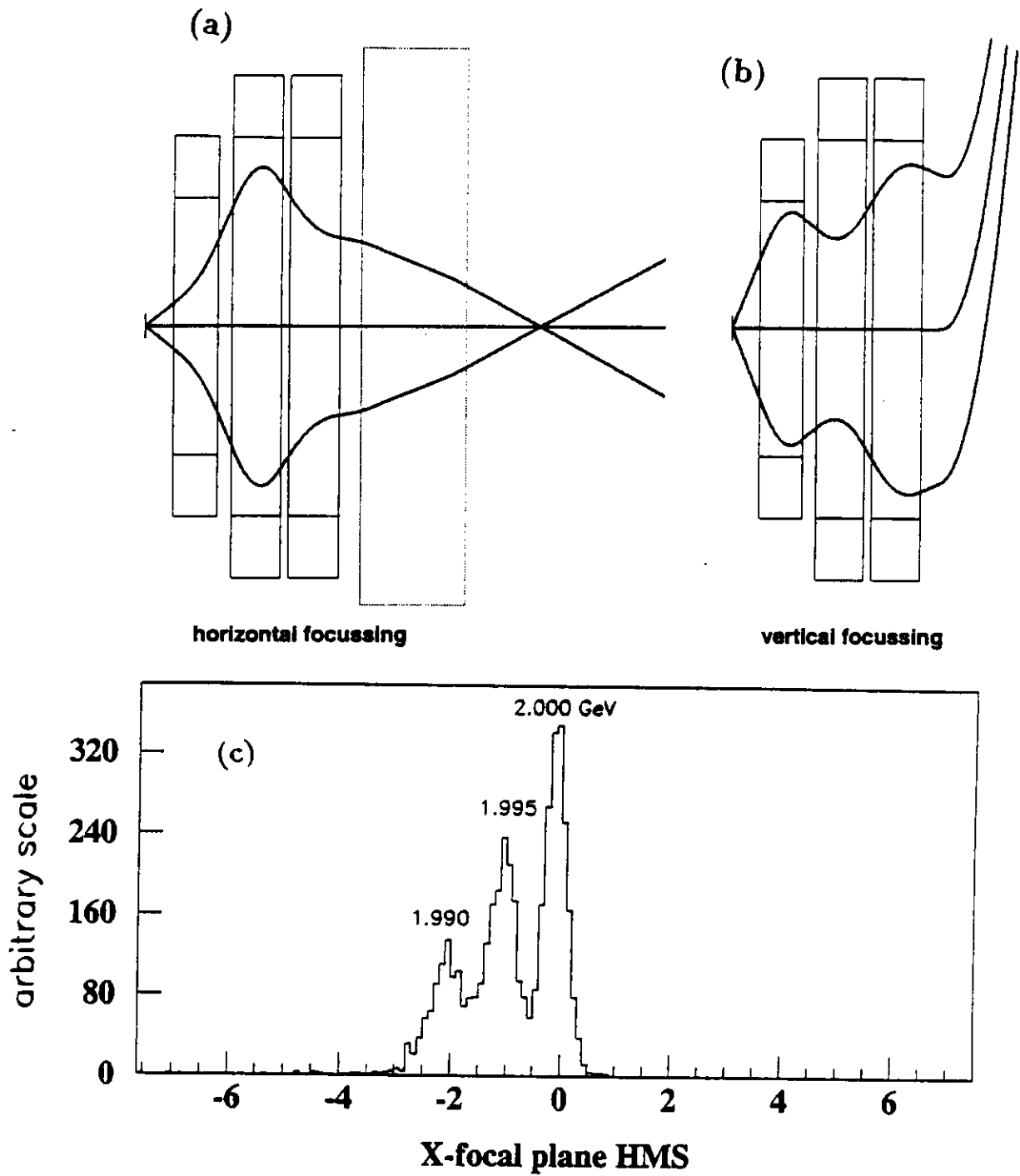


Figure 4.7: (a)–(b) Using TOSCA field maps in GEANT, the expected trajectories are indicated through the magnets. (c) Inelastic scattering off  $^{12}\text{C}$  at 2 GeV.

In estimating the coincidence rate  $R_c(e, e'K)$ , we use [35]

$$R_c(e, e'K) = \frac{I}{e} \cdot \frac{\rho t N_0}{A} \cdot \frac{d^3\sigma}{dE_e d\Omega_e d\Omega_K} \cdot \Delta E_e \Delta\Omega_e \Delta\Omega_K \cdot (1 - P_{\text{decay}}) \quad (4.1)$$

with  $t = 5$  cm (target length),  $\Delta\Omega_e = 5$  msr,  $\Delta\Omega_K = 4$  msr,  $\Delta E'_e = 0.2E'_e$ , where  $\Delta\Omega$  is the solid angle of the spectrometer, and  $(1 - P_{\text{decay}})$  is the kaon survival probability over a 10-m flight path. The beam currents ( $I = 20\text{--}60 \mu\text{A}$ ) have been chosen to maximize the signal to noise ratio.  $R_e(e, e')$  and  $R_K(e, K)$  are the singles rates in the HMS and SOS arms respectively. The ratio of accidental to true is given by

$$\frac{A}{T} = \frac{\tau \cdot R_e \cdot R_K}{f \cdot R_c}$$

where  $\tau = 2$  ns resolving time and  $f = 1$  duty factor have been used. The contribution  $\sigma(\gamma_{\nu n} \rightarrow K^+\Sigma^-)$  for the neutron in deuterium was conservatively taken to be the same as  $\sigma(\gamma_{\nu p} \rightarrow K^+\Sigma^0)$ . Table 4.3 lists the computed rates for the kinematics conditions given in Table 4.1.

Table 4.3: Coincidence and single rates for  $d(e, e'K^+) \Lambda \Sigma^0$  or  $\Sigma^-$

Kine.	I ( $\mu\text{A}$ )	$R_c(e, e'K)$ ( $10^{-2}$ Hz)	$R_e(e, e')$ (kHz)	$R_K(e, K)$ (kHz)	A/T ( $\tau = 2$ ns)	Time (hours)
1.a	10	6.5	5.3	1.33	0.22	26
1.b	10	19.1	24.0	1.22	0.30	9
1.c	5	19.0	28.2	0.59	0.17	9
2.a	40	4.28	0.80	6.64	0.24	39
2.b	20	7.2	2.78	2.70	0.20	23
2.c	30	15.4	7.5	2.10	0.24	11
3.a	60	1.12	0.18	4.68	0.16	149
3.b	60	3.88	1.40	3.80	0.28	43
3.c	40	5.5	2.62	2.26	0.21	30
4.a	60	1.88	0.12	17.0	0.20	89
4.b	60	2.88	0.24	14.9	0.24	58
4.c	60	4.94	0.56	12.7	0.28	34

## 4.4 Run time

Our beam time request is based on obtaining a statistical uncertainty of  $1\frac{1}{3}\%$  at each measured point. The events which pass the hardware trigger (and are taken to tape) will contain some background events from random coincidences. The good S/N ratio (shown in Table 4.3) means that the correction to this is small. Corrections due to finite detector acceptance also will be done off-line. The beam time required to obtain reasonable statistics is summarized in Table 4.4. A total of 27 days of running is requested.

To minimize overhead, all data at one incident energy will be taken, changing the spectrometer angles appropriately. The pion and proton background shapes will be determined by prescaling a portion of the  $(e, e'\pi^+)$  and  $(e, e'p)$  yields.

Table 4.4: **Beam Time Request**

	<b>TIME (DAYS)</b>
<b>Data Acquisition</b>	<b>21.7</b>
<b>Setup and Checkout</b>	<b>1.0</b>
<b>Angle Changes</b>	<b>0.8</b>
<b>Normalization Studies</b>	<b>1.5</b>
<b>Energy Changes</b>	<b>2.0</b>
<b>TOTAL</b>	<b>27.0</b>

## 4.5 Response to PAC 8 comments

This proposal was deferred by PAC 8 in June of 1994. The questions and criticisms of the PAC 8 review are summarized here, along with the further work done to answer their questions. The main criticism of PAC 8 was that although the PAC found  $(e, e'K^+)$  studies an important part of the CEBAF program, a clearly focused physics motivation for the experiment was not presented.

In particular, the PAC asked for an assessment of the experiment's impact on 1) the determination of the neutron amplitudes, 2) the extraction of the  $\Lambda n$  interactions, and 3) the extraction of the kaon form factor. Finally, a simulation of the detector response to estimate systematic errors was requested.

Although a neutron target would be preferable to determine the neutron amplitudes, the use of deuterium is acceptable, as discussed in Chapter 2. The modifications of the  $\gamma_{\nu}p \rightarrow K^+\Lambda$  channel provide a calibration for modifications to the  $\gamma_{\nu}n \rightarrow K^+\Sigma^-$  channel. At the same time, these modifications of the  $\Lambda$  also present the simplest means of extracting the  $\Lambda n$  interactions, as discussed in Chapter 3. The collaboration intends to submit a future proposal examining modifications in heavier nuclei, after the first round of kaon electroproduction experiments (E93-018 and E91-016) have been performed.

The extraction of the kaon form factor is not the goal of this experiment. Knowledge of the kaon form factor is best obtained by use of a hydrogen target, as will be done in E93-018. This experiment will study the mechanisms of kaon electroproduction off the simplest nuclear target. Interpretation of the reaction in these terms is in itself a challenging task, as discussed in Chapters 2 and 3.

Chapter 4 contains a section devoted to explaining how the response of the detectors has been simulated, using the GEANT Monte Carlo code. Both the HMS and SOS have been input into the code, including all relevant detectors. The analysis of the data has been fully simulated by using the same software routines to analyze the simulations that the experiment will use.

PAC 8 also asked the collaboration to explore performing the experiment in conjunction with E93-018 to minimize systematic uncertainties. [E93-018 is run with a hydrogen target at identical kinematics.] However it is the choice of Hall C detectors and kinematics which is critical for this experiment. Although this experiment would like to run as soon as possible (ideally in conjunction with E93-018), the systematic uncertainty is minimized by using the same detectors, data handling, binning, PID and analysis routines, in order to accurately compare to the hydrogen data.

# References

- [1] Joseph Cohen . *Phys. Lett.*, **153B** 367, 1985.
- [2] T. E. Rudy, H. W. Fearing and S. Scherer . *TRI-PP-94-4*, 1994.
- [3] Robert A. Williams et al. . *Phys. ReV.*, **C46** 1617, 1992.
- [4] F. M. Renard and Y. Renard . *Phys. Lett.*, **24B** 159, 1967.
- [5] C. B. Dover, D. J. Millener, A. Gal . *Physics Report*, **184** 1, 1989.
- [6] R. S. Hayano . *Nucl. Phys.*, **A527** 477c, 1991.
- [7] B. Mecking (Spokesman) . *CEBAF Experiment E-89-045*.
- [8] B. Zeidman (Spokesman) . *CEBAF Experiment E-91-016*.
- [9] R. Adelseck, Ohio State University . *Final-state hyperon-nucleon interaction in kaon photoproduction from deuteron*, 1988.
- [10] Shian S. Hsiao and Stephen R. Cotanch . *Phys. Lett.*, **163B** 300, 1985.
- [11] Steven R. Cotanch and Shian S. Hsiao . *Nucl. Phys.*, **A450** 419c, 1986.
- [12] Steven R. Cotanch and Shian S. Hsiao . *SLAC-316, UC-34C (T/E)*, 1987.
- [13] C. J. Bebek et al. . *Phys. Rev.*, **D15** 594, 1977.
- [14] A. M. Boyarski et al. . *Phys. Lett.*, **34B** 547, 1971.
- [15] D. J. Quinn et al. . *Phys. Rev.*, **D20** 1553, 1979.
- [16] Shoji Shinmura . , *Electroproduction of Light  $\Lambda$ - and  $\Sigma$ -Hypernuclei*, Gifu University, 1994.
- [17] P. Brauel et al. . *Z. Physik. C, Part. and Fields*, **3** 101, 1979.
- [18] R. C. E. Devenish et al. . *Phys. Rev.*, **D5** 47, 1972.
- [19] O.K. Baker (Spokesman) . *CEBAF Experiment E-93-018*.

- [20] P. Brauel et al. . *Phys. Lett.*, **69B** 253, 1977.
- [21] R. D. Reid . *Ann. of Phys.*, **50** 411, 1968.
- [22] T. Hamada and I. D. Johnson . *Nucl. Phys.*, **34** 382, 1962.
- [23] C. Bennhold . *Nucl. Phys.*, **A547** 79c, 1992.
- [24] O. Nachtmann . *Nucl. Phys.*, **B115** 61, 1976.
- [25] G. R. Farrar et al. . *Nucl. Phys.*, **B349** 655, 1991.
- [26] R. L. Anderson et al. . *Phys. Rev.*, **D14** 679, 1976.
- [27] CCFR Collaboration . *Phys. Rev. Lett.*, **64** 1207, 1990.
- [28] H. Deden et al. . *Nucl. Phys.*, **B85** 269, 1975.
- [29] T. S. H. Lee, ANL, (private communications) .
- [30] S. Beedoe and O. K. Baker, GEANT Simulation of the Hall C Spectrometers, Hampton University .
- [31] C. Yan et al. . *CEBAF-R-92-002*.
- [32] CEBAF Conceptual Design Report (CDR) . 1990.
- [33] C. J. Bebek et al. . *Phys. Rev.*, **D15** 3082, 1977.
- [34] L. W. Lightbody and L. S. O'Connell . *Comp. Phys. May/June*, page 57, 1988.
- [35] T. Angelescu, Bucharest University (private communications) .